Analysis of DNA Replication by Optical Mapping in Nanochannels

Joris Lacroix, Sandrine Pélofy, Marie-Charline Blatché, Marie-Jeanne Pillaire, Sébastien Huet, Catherine Chapuis, Jean-Sébastien Hoffmann, Aurélien Bancaud

Analysis of DNA replication by optical mapping in nanochannels

Joris Lacroix[1,2], Sandrine Pélofy[1,2], Charline Blatché[1,2], Marie-Jeanne Pillaire[5,2], Sébastien Huet[3,4], Catherine Chapuis[3,4], Jean-Sébastien Hoffmann[5,2], Aurélien Bancaud[1,2]

[1] CNRS, LAAS, 7 avenue du colonel Roche, F-31400 Toulouse, France

[2] Univ de Toulouse, LAAS, F-31400 Toulouse, France

[3] CNRS, UMR 6061, Institut Génétique et Développement de Rennes

[4] Université Rennes 1, UEB, UMR 6290, Faculté de Médecine, Rennes F-35043, France

[5] Equipe «Labellisée LA LIGUE CONTRE LE CANCER 2013» - Laboratoire d'Excellence Toulouse Cancer LABEX TOUCAN - Cancer Research Center of Toulouse, Inserm U1037, CNRS ERL5294, 2 Avenue Hubert Curien, CS 53717, 31037 Toulouse, France

Correspondence: abancaud@laas.fr

Running title: DNA replication analysis in nanochannels

Keywords: DNA replication, optical mapping, nanochannels, chromosome manipulation, single DNA molecule microscopy

Abstract

DNA replication is essential to maintain genome integrity in S phase of the cell division cycle. Accumulation of stalled replication forks is a major source of genetic instability, and likely constitutes a key driver of tumorigenesis. The mechanisms of regulation of replication fork progression have therefore been extensively investigated, in particular with DNA combing, an optical mapping technique that allows the stretching of single molecules and the mapping of active region for DNA synthesis by fluorescence microscopy. DNA linearization in nanochannels has been successfully used to probe genomic information patterns along single chromosomes, and has been proposed to be a competitive alternative to DNA combing. Yet this conjecture remains to be confirmed experimentally. Here we establish two complementary techniques to detect the genomic distribution of tracks of newly synthesized DNA in human cells by optical mapping in nanochannels. We compare their respective advantages and limitations, and apply them to detect deregulations of the replication program induced by the antitumor drug hydroxyurea. Our developments thus broaden the field of applications accessible to nanofluidic technologies, and could be used in the future as part for molecular diagnostics in the context of high throughput cancer drug screening.

Introduction

DNA replication, which occurs just before cell progress into mitosis, is one of the most regulated and concerted process within cell cycle. It initiates at replication origins from which replication forks proceed bi-directionally, allowing an accurate and rigorous duplication of the genomic material that insures transmission of the genome integrity in successive cell generations. There is a single origin of replication on the *Escherichia coli* chromosome [1] and this number increases with the size of the genome from ~400 in the yeast *S. Cerevisiae* to 30-50 thousands in human cells distributed with an average interval of 100 kb [2]. The firing of these origins is regulated temporally [3], and this timing program is deregulated in many disease states, including cancer [4]. Therefore the characterization of the dynamics of DNA replication in living cells and/or in cell-free systems constitutes a major challenge in biology. Among the techniques to map the replication program, DNA combing allows the visualization of newly synthesized DNA at the single molecule level [5,6]. This technique, which met considerable success in academic environment, consists in adsorbing and aligning single DNA molecules onto microscope coverslips using the spreading forces exerted by a receding meniscus. Elongated molecules are then observed by fluorescence microscopy in order to map the genomic distance between tracks of newly-synthesized DNA at a maximal resolution of ~700 bp [7]. DNA combing suffers from intrinsic limitations mainly associated to the random placement of molecules on the surface, and to the critical quality of the surfaces onto which fibers are stretched [8].

Micro- and Nano-technologies have been employed to enhance the throughput of DNA combing. The placement of elongated molecules in ordered arrays has been achieved using surface patterning [9] or arrays of micro-channels of 8 µm in height [10]. Single chromosome fragments have also been elongated after partial immobilization on a charged glass surface in a microfluidic flow cell [11]. After sequence-specific enzymatic digestion, genome restriction maps have been produced in bacteria [12], human [13], and goat with this technique [14]. Alternatively, using shallow channels of ~100 nm in cross section, the steric constraints imposed by the walls on single DNA molecules have been exploited to force their longitudinal elongation [15,16]. This method, which is often referred to as optical mapping in nanochannels [17], has been optimized for continuous genomic analysis based on the control of the flux of molecules entering in nanochannels [18]. Potentially relevant to high throughput replication analysis, this technology has been predominantly applied to produce genomic barcodes based on enzyme recognition sites [19] or GC-content along partially-denaturated molecules [20]. Genome-wide measurements for the identification of bacterial cells [21] or the detection of chromosome rearrangements in human cells [22] have been reported.

Here we establish two complementary methods to investigate DNA replication by optical mapping in nanochannels (Fig. 1A). Newly synthesized DNA is detected either with a fluorescent nucleotide analog (dUTP-Cy3) incorporated in the genome during replication, or by titration of the DNA content along a single chromosome fiber using the DNA intercalating fluorophore SYTOX-Orange. We demonstrate the consistency of the readouts obtained with these two methods, and come to the conclusion that the second approach is easier to implement and significantly more work-effective. We finally show that optical mapping in nanochannels can be used to monitor replication stress induced by hydroxyurea, a drug that stalls the progression of replication forks through the depletion of deoxyribonucleotides. We finally discuss the relevance of our developments in comparison to DNA combing, in particular in the context of drug screening and/or diagnostic applications.

Results and discussion

Process flow for DNA replication analysis in nanochannels

We set up two methods to probe DNA replication, as depicted in Fig. 1A. In both cases, U20S osteosarcoma cells were treated by addition of 0.5 µM aphidicolin during 16 h in order to increase the proportion of cells in S phase to 73% versus 43% in untreated conditions, as inferred from fluorescence assisted cell sorting (FACS, Supplementary Fig. S1). Cells were then placed in fresh medium during 3 or 6 hours at 37°C to resume replication. In method 1, stable incorporation of dUTP-Cy3 into the genome was achieved by forcing the entry of this label into the cells by scraping them with a rubber, as described in ref. [23,24]. Cells were harvested by trypsinization the day after, and encapsulated in agarose for chromosome extraction. 3 hours after aphidicolin release, cells were directly harvested in method 2 and encapsulated in agarose for extraction of genomic DNA.

After agarose enzymatic digestion, the genomic material was stained with the DNA intercalating fluorophores SYTOX-Orange or YOYO-1. Chromosome structural inspection by linearization in nanochannels was carried out in poly-dimethysiloxane nanochannels of 250*200 nm^2 in rectangular cross section and 100 µm in length (Fig. 1B, see methods section and ref. [25] for details). Chromosome fragments were continuously conveyed through nanochannels by hydrodynamics at a velocity of 200 +/- 20 µm/s, following the manipulation method described in [26]. They were observed by fluorescence microscopy at an inter-frame interval of 40 ms, which included an exposure time of 15 ms and a transfer time of 25 ms. Molecules were analyzed ‘on the fly’ at the onset of the nanochannel because the degree of elongation is enhanced with hydrodynamic actuation [26].

Optical mapping of Cy3 labeled newly-synthesized DNA (Method 1)

Successful incorporation of dUTP-Cy3 was first validated in living cells by monitoring the presence of discrete, mostly diffraction-limited, foci by fluorescence microscopy (Fig. 2A). The fraction of Cy3- positive cells was 70 +/- 15%, according to the percentage of cells in S phase measured by FACS (Supplementary Fig. S1), but the survival rate after the scraping step spanning 10 to 40% was modest. Chromosomes were extracted and characterized by DNA combing, which was used as benchmark technique (Fig. 2B). Along linear DNA fibers stained with YOYO-1, we observed tracks of dUTP-Cy3 of 23.5 +/- 6.6 µm (n=115, Fig. 2C), which exhibited polarized intensity distributions (Fig. 2B). In order to estimate the genomic length of these tracks, we considered the stretching factor of 0.45 µm/kb determined with combed λ-DNA (48.5 kbp) on amino-coated surfaces [27], and deduced that dUTP-Cy3 tracks measured 52 +/- 14 kbp. Given the speed of DNA replication forks of ~2 kbp/min [28], we evaluated that dUTP-Cy3 incorporation occurred during ~30 minutes. This time scale appeared to be consistent with our live cell observations on the formation of dUTP-CY3 foci after microinjection, which took place in ~30 minutes (S.H. unpublished results). In addition, we suggest that the polarity of dUTP-Cy3 tracks is accounted for by the progressive consumption and/or degradation after the mechanical formation of pores by scraping.

dUTP-Cy3 tracks were subsequently analyzed by optical mapping in nanochannels. We first recorded the passage of dUTP-Cy3 loci with single color wide field microscopy (Fig. 2D). The physical size of dUTP-Cy3 tracks was 15 +/- 5 µm (n=40; Fig. 2E). In order to relate this measurement to that of DNA combing, we had to estimate the stretching factor in nanochannels. We prepared concatemers of λ-phage DNA (see methods) and measured the extension of molecules containing 1 to 4 copies of λ-DNA at the entry of nanochannels (Supplementary Fig. S2A). This calibration allowed us to determine the stretching factor of 0.3 µm/kb, implying that the average size of dUTP-Cy3 tracks of 50 +/- 15 kbp was consistent with our DNA combing data (Fig. 2F). Note that the stretching factor corresponds to 80 +/- 10% of DNA contour length, consistent with DNA elongation response in nanochannels [29] that varies marginally for forces larger than ~1 pN. Furthermore we confirmed our observation on the polarity of the tracks, as for instance shown in Fig. 2G. We then scored inter-track distances, which were inferred from the distance between the center of mass of consecutive tracks. Inter-track appeared to be broadly distributed with a mean 120 kb and a standard deviation of 35 kb (n=32). Furthermore the histogram was skewed toward long intervals, in agreement with the non-Gaussian behavior observed in most DNA combing studies [30].

We also intended to monitor the passage of chromosome fragments labeled with YOYO-1 and dUTP-Cy3 simultaneously in order to improve the quality of this measurement technique. In our hands, however, the signal-to-noise ratio of dUTP-Cy3 tracks was degraded in dual color wide field microscopy, seriously challenging the mapping of inter-track distances. Using confocal microscopy, tracks of weak intensity in the Cy3 spectral window were detected along chromosomes (Supplementary Fig. S2B), the size of which was consistent with DNA combing and optical mapping observations. However these tracks were spatially concomitant with 3-fold intensity onsets in the YOYO-1 channel. This result was somewhat surprising given the separate emission-excitation spectrum of the two fluorophores, and raised concerns about the feasibility of the determination of chromosome fragment size using dUTP-Cy3 incorporation method. Consequently, although our experiments showed that newly-synthesized DNA labeled with Cy3 could be detected by optical mapping in nanochannels, the modest survival rate and the limitations of dual color microscopy led us to consider an alternative, yet mutually reinforcing, technique for DNA replication analysis.

Optical mapping of SYTOX-labeled chromosomes (Method 2)

DNA replication has been studied using surface-immobilized DNA, and replication bubbles have been detected by measuring the DNA content along the contour of individual molecules with the fluorescent probe SYTOX-Orange [31,32]. Hence we used this fluorophore to stain genomic DNA and map fluorescence intensity patterns at the single molecule level. We expectedly detected the passage of chromosome fragments with telegraphic intensity modulations likely associated to the doubling of fluorescence intensity in tracks of newly synthesized DNA (Fig. 3A). Similar intensity patterns were also detectable with DNA combing (Supplementary Fig. S2C).

We focused our investigations on chromosomes purified 3 hours after aphidicolin release, and specifically analyzed long fragments of more than 100 µm (Fig. 3B). We recorded a time series of ~45 minutes with an inter-frame interval of 40 ms, and scored the fraction of patterned molecules passing through nanochannels, which represented 46 +/- 5% of the genomic sample of ~45 Mbp. We also observed that this fraction dropped to ~7 % for chromosomes purified 6 hours after aphidicolin release (not shown), *i.e.* at the end of the replication program. This result strongly supported the fact that intensity patterns on single molecules were associated to replication tracks. We then evaluated the physical length of SYTOX tracks and the distance between the center of mass of consecutive tracks, which were characterized by broad distributions with average sizes of 38 +/- 13 µm (n=38) and 46 +/- 14 µm (n=20), respectively (Fig. 3C). Notably intensity patterns, which are inferred “on the fly”,

are blurred due to the travel of the molecule in the course of the acquisition, and we show that tracks of less than ~5 µm are underscored in Supplementary Fig. S2D.

We then wished to translate these results into genomic distances. Given that chromosome fragments were analyzed at the entry of nanochannels, we used the same stretching factor of 0.3 µm/kb as for the analysis of dUTP-Cy3 tracks. The track length was therefore 126 +/- 40 kbp and the distance between the center of mass of consecutive tracks was 150 +/- 45 kbp on patterned molecules. Considering the breadth of the distributions of replication tracks, this result was comparable to our measurement obtained with dUTP-Cy3 of 120 +/- 35 kbp. Overall dUTP-Cy3 and SYTOX labeling methods appeared to yield consistent results, yet the simple sample preparation procedure with SYTOX led us to focus on this technology to demonstrate that optical mapping could be used to detect defects in the replication program under replication stress.

Monitoring replication stress induced by hydroxyurea by optical mapping

Hydroxyurea (HU) is a DNA replication inhibitor, which affects DNA synthesis by depletion of deoxyribonucleotides, resulting in stalled replication forks [33] which, after prolonged treatment, collapse into double-strand breaks [34]. 3 hours after aphidicolin release (Fig. 4A), cells were exposed to 2 mM HU during 3 hours, their genomic DNA was then purified, and optical mapping in nanochannels was carried out in control *vs*. HU treated cells. This analysis was carried out on ~35 Mbp of genomic DNA, and it indicated that HU treatment was associated to an onset of the fraction of patterned molecules to 30 +/- 5%. In fact patterned molecules became consistently detectable upon drug addition whereas they could hardly be seen in the control with a fraction of ~7%. This result was in agreement with the fact that HU stalls the replication forks. In addition we noticed that the distribution of track lengths was 52 +/- 13 µm, equivalently 173 +/- 40 kbp (Fig. 4B), hence 40% greater than that the average after three hours under normal conditions for replication (Fig. 3C, note that we could not evaluate the track length distribution after 6 hours due to the low number of patterned molecules). Inter-track also increased to ~90 µm (n=6) although we could not precisely sample the distribution for such long genomic distances of ~300 kbp. Because HU slows down the progression of the replication fork, we could detect replication tracks upon addition of the drug whereas tracks likely become overly long to be detected given our technological settings. Consequently, although improvements could be made to improve track detection for features smaller than 5 µm or greater than ~100 µm, our technological development enabled us to detect the consequences of replication stress induced by HU on human cancer cells.

Discussion and conclusion

We have described a novel method at the frontiers of molecular biology and nanotechnology to characterize the process of DNA replication by optical mapping in nanochannels. Its development has required the setting up of non conventional methods to label newly synthesized DNA. For instance whenever DNA was stained with YOYO-1 instead of SYTOX Orange, patterns became indiscernible, likely because the cross-links mediated by this bis-intercalating dye [35] biased DNA content titration in replication bubbles. In addition the standard labeling technique in DNA combing involves immunostaining using antibodies that target synthetic nucleosides such as the thymidine analog BrdU (5-bromo-2'-deoxyuridine). The antibody reacts with BrdU in single stranded DNA [36]. Yet single stranded DNA has been seldom manipulated in nanochannels due to its low persistence length of ~3 nm *vs*. ~50 nm for double stranded DNA, because linearization is only achieved in highly confined canalizations. Alternatively the cell-permeable alkynyl nucleoside analog EdU (5-ethynyl-2'-deoxyuridine), which allows direct labeling of newly synthesized DNA by Click-chemistry [37], was incompatible with optical mapping in our hands. Oxidative DNA damage, which is coincident with the Click-reaction [38], indeed leads to chromosome fragmentation (Supplementary Material and Fig. S3). Notably the variety of synthetic nucleoside available on the market is readily suited to carry out pulse chase labeling, which has been ubiquitously used to measure the dynamics of replication forks. We did not show multi-color labeling in this report, mostly because cell re-adhesion after the scraping step takes ~4 hours, hence forbidding consecutive operations. We thus suggest that additional labeling methods, based on e.g. electroporation or lipotransfection, should be implemented to enhance the potential of nanofluidics for basic research.

Despite this limitation, optical mapping in nanochannels may have key advantages over DNA combing. First DNA combing results critically depend on the quality of the surfaces onto which fibers are stretched [8], because the background signal of immunofluorescence detection can be challenging to reduce for single molecule detection. Conversely DNA is repelled from surfaces for its manipulation in nanochannels using polymer coating (see methods section), and labeling is carried out in bulk, allowing us to carefully titrate the DNA:fluorophore ratio (method 2). Moreover, the detection of linearized molecules in DNA combing imposes the scanning over entire glass coverslips, whereas chromosomes are conveyed to the nanochannel array for their analysis by optical mapping. The nanofluidic chip can thus be used for continuous acquisitions, which are more favorable for large datasets acquisition. Finally this technology is readily suited to the manipulation of cell samples comprising small numbers of cells. In this report the vial for molecular analysis contained 30 000 cells diluted in 800 µL, and we conveyed approximately 10% of this solution in the chip, implying that the sample contained ~3000 cells. Further efforts to analyze 1-10 cells are underway [39], and they mostly

require the engineering access microchannels rather than modification of the strategy of DNA manipulation in nanochannels. Consequently, although DNA combing has demonstrated its relevance for unveiling detailed cellular events that take place during fork progression under normal growth conditions or after replication stress, developments of specific assays and calibration schemes for optical mapping in nanochannels may have advantages for translational and clinical research. For example, the establishment of DNA replication profiles has been proposed to be relevant for cancer therapy, since several widely used anticancer drugs, such as cisplatin, cytarabin, or fludarabin, target replication forks [40]. However, the determination of DNA replication parameters, such as fork velocity and origin activity, in a large cohort of patients remains a challenge. For this challenge to be overtaken, several technological parameters should be optimized. For instance, the lateral size of nanochannels, which defines DNA stretching factor, may be specified in order to reach genomic resolutions of 400-bp, as was shown in 100 nm nanochannels [15]. Furthermore chromosome preparation should be optimized so as to manipulate fragments of several Megabp in the fluidic chip. Given that such resolution in size is hardly accessible to DNA combing, our technological contribution may be a serious option to elucidate whether cancer molecular signatures can be obtained from DNA replication analysis.

Material and Methods

All reagents were purchased from Sigma-Aldrich unless mentioned.

Cell culture

The human osteosarcoma U2OS cell line was grown in 6-well plates to ~80% confluence. They were synchronized at the G1/S transition using aphidicolin at a concentration of 0.5 µM during 16 h. After aphidicolin release, cells were placed in fresh medium during 3 hours at 37°C to resume replication. At this stage, cells were harvested either for extraction of genomic DNA, or for labeling the newly synthesized DNA through dUTP-Cy3 incorporation. The latter method consisted in filling each well with 100 µL of phosphate saline buffer (PBS) supplemented with 10 µM dUTP-Cy3, this concentration representing ~1/3 of physiological dNTP levels [41]. Cells were scraped with a silicone rubber, and they were left during 30 minutes in this solution at 37°C before addition of 2 mL of medium during 5 hours at least.

Extraction of genomic DNA

Cells were trypsinized, counted, and centrifuged at 1400 rpm during 5 minutes. They were resuspended in PBS at a concentration of 1000 cells/µL. This solution was mixed in equal proportion with low melt agarose (BioRad) dissolved in PBS at a concentration of 1.6% (w:v). 100 µL of this solution was dispensed in parallelepiped-shaped teflon vials, then placed at 4°C during 30 minutes in order to trigger agarose reticulation. Genomic DNA was then purified by soaking the agarose plugs in TE buffer (10 mM Tris-HCl, 1 mM EDTA, pH=7.5) supplemented with 10% SDS and 250 µg/mL proteinase K (Fisher) during 48 h at 37°C. Agarose plugs were eventually rinsed in TE and stored at 4°C. We also prepared λ-phage DNA concatemers that were obtained by overnight ligation of a monomer solution at 50 ng/µL in the presence of 5% poly-vinylpyrrolidone (40 kDa).

Nanochannel fabrication

The mold for chip fabrication was generated using a combination of conventional photolithography and phase-shift lithography for printing micro- and nano-patterns, respectively. These patterns were then transferred into silicon with reactive ion etching (see ref. [25] for details). The resulting reliefs for nanochannels measured 250*200 nm^2 in cross section and 100 µm in length (Fig. 1B). The nanofluidic chips for DNA replication analysis were produced by pouring and spin-coating a thin layer of 40 µm of a rigid silicone elastomer (poly-dimethylsiloxane (PDMS) of Young modulus of 5 MPa). This material was reticulated during 45 minutes at 75°C, and it was then covered by a thick layer of standard PDMS (Sylgard 184) of ~1 cm baked during 3 hours at 75°C. Access holes were punched through the resulting PDMS chips, and they were assembled on microscope coverslips using surface activation by oxygen plasma (200 W, 30 s).

Genomic DNA manipulation

Each experiment was carried out with the third of an agarose plug, which was deposited in a tube of 1.5 ml. The tube was then filled with 800 µL of 0.5X TBE buffer supplemented with 2% poly-vinylpyrrolidone (40 kDa, below the overlapping concentration of 7%) and 5% dithiothreitol (DTT) or in 800 µL of 1X TE for optical mapping or DNA combing experiments, respectively. Agarose was melted by heating the tube at 60°C during 10 minutes. The temperature was set to 42°C, and 2 µL of β-agarase (Fisher) was added for overnight agarose digestion. Finally DNA was stained with the fluorophores YOYO-1 or SYTOX-orange (Molecular Probes) at an approximate ratio of 1 dye per 5 pb.

Chromosome structural characterization was conducted with DNA combing using the protocol described in ref. [42]. The pH was set to 7.5 and glass slides were modified with (3-aminopropyl)-triethoxysilane (surface modification protocol described in ref. [43]). For optical mapping, we used hydrodynamics to force the uptake of chromosomes in nanochannels. The velocity of molecules was set to 200 +/- 20 µm/s using a pressure source at ~300 mbar.

Imaging was performed with a wide-field inverted microscope equipped with a 40X lens (NA=1.4). The light source was a LED engine (Lumencor) emitting at 470/24 nm or 542/33 nm with the filter sets LF488/LP and Cy3-4040C (Semrock) for YOYO-1 and Cy3/SYTOX visualization, respectively. Images were collected with an Andor EM-CCD camera operating with an inter-frame interval of 40 ms with a 2x2 binning (pixel size = 400 nm).

Image treatment

All images presented in the manuscript were filtered using the FFT bandpass filter implemented in ImageJ using minimum and maximum cut-offs of 3 and 40 pixels, then background subtracted.

Figure 1: DNA labeling methods for replication analysis by optical mapping in nanochannels. (A) The scheme represents the two processes for chromosome extraction and labeling. In each method, the dashed line corresponds to the step of genomic DNA extraction. **(B)** The central image in the panel sketches the chip for chromosome fragment manipulation. On the right side, we present scanning electron micrographs of the silicon mold, which is used for chip fabrication, with magnifications of 10000 and 25000 (red and green borderlines, respectively). The thickness of the two access microchannels is 2 µm and nanochannels measuer 200 nm in height. DNA molecules are linearized when they enter in nanochannels, as shown in the fluorescence micrograph at the right, which present λ-DNA concatemers labeled with YOYO-1 in the course of their migration through nanochannels.

Figure 2: Newly-synthesized DNA labeled with dUTP-Cy3 (method 1 of Fig. 1A). (A) The fluorescence micrograph shows dUTP-Cy3 foci in a U2OS cell one day after scrape loading. **(B)** After chromosome extraction, DNA combing allows us to detect polar dUTP-Cy3 tracks along DNA fibers labeled with YOYO-1. **(C)** The histogram represents the physical size of dUTP-Cy3 tracks as inferred from DNA combing (*n* corresponds to the number of events in the histogram). **(D)** The time series represents the passage of one dUTP-Cy3 track in a nanochannel of 200 nm in cross section. The signal to noise ratio of the track, as defined by the maximum intensity divided by the variance of the background signal, is equal to 7. **(E)** The histogram shows the size distribution of dUTP-Cy3 tracks obtained by optical mapping in nanochannels. **(F)** The plot shows the comparison of genomic size distributions of dUTP-Cy3 tracks inferred from DNA combing and optical mapping (line and histogram, respectively), after calibration of the stretching factor in each technique (see main text). **(G)** The fluorescence micrograph corresponds to one chromosome fragment containing three dUTP-Cy3 tracks, which are indicated by green arrowheads. Polar fluorescence intensity is detected for the track in the middle, in agreement with our observation of DNA combing. The inter-track genomic distance distribution obtained by optical mapping is represented below.

Figure 3: DNA titration with SYTOX-Orange for replication analysis (method 2 in Fig. 1A). (A) The upper schematic depicts the passage of a chromosome fragment with two replication bubbles. The lower panel shows the time series of one SYTOX labeled chromosome fragment with telegraphic intensity variations, which are characterized by a SNR of 2.5. The green arrowheads show the consecutive positions of one track within one long molecule of ~400 kbp in the course of its progress through the nanochannel. **(B)** The histogram represents the genomic size of 46 fragments analyzed by

optical mapping in nanochannels (*n* corresponds to the number of events in the histogram). **(C)** The genomic size of replication tracks (track length) and inter-track genomic distances are scored 3 hours after aphidicolin release.

Figure 4: Monitoring replication stress induced by HU treatment. (A) Schematics of the protocol for HU treatment. **(B)** The two graphs represent the genomic size of SYTOX tracks and their consecutive distances in the control *vs*. HU treated cell sample (line vs. histogram plots, respectively), as inferred from method 2 (see e.g. Fig. 3A).

Acknowledgments: We thank Philippe Pasero for critical reading and suggestions on the manuscript, and Serge Mazères for assistance in confocal microscopy. This work was supported by the "Plan Cancer" grant (One-Chip) and the ANR grant JC08_341867. This work was also supported by the LAAS-CNRS technology platform, a member of the French Basic Technology Research Network. J.L. thanks the RITC network for PhD fellowship.

Author contribution: J.L., S.P., C.B., C.C. designed the study, fabricated nanodevices, and performed data analysis. M.J.P., S.H., J.S.H. wrote the paper. A.B. designed the study, and wrote the paper.

Bibliography

[1] A. Kornberg, T. A. Baker, *DNA Replication*, Freeman, W. And Co., New York, **1992**.
[2] C. Alabert, A. Groth, *Nat Rev Mol Cell Biol* **2012**, *13*, 153.
[3] M. Méchali, *Nat. Rev.* **2001**, *2*, 640.
[4] N. Donley, M. J. Thayer, *Semin Cancer Biol* **2013**, *23*, 80.
[5] A. Bensimon, A. Simon, A. Chiffaudel, V. Croquette, F. Heslot, D. Bensimon, *Science* **1994**, *265*, 2096.
[6] X. Michalet, R. Ekong, F. Fougerousse, S. Rousseaux, C. Schurra, N. Hornigold, M. van Slegtenhorst, J. Wolfe, S. Povey, J. S. Beckmann, A. Bensimon, *Science* **1997**, *277*, 1518.
[7] G. Versini, I. Comet, M. Wu, L. Hoopes, E. Schwob, P. Pasero, *Embo J* **2003**, *22*, 1939.
[8] H. Labit, A. Goldar, G. Guilbaud, C. Douarche, O. Hyrien, M. Marheineke, *BioTechniques* **2008**, *45*, 649.
[9] A. Cerf, B. R. Cipriany, J. J. Benitez, H. G. Craighead, *Anal Chem* **2011**, *83*, 8073.

[10] E. T. Dimalanta, A. Lim, R. Runnheim, C. Lamers, C. Churas, D. K. Forrest, J. J. de Pablo, M. D. Graham, S. N. Coppersmith, S. Goldstein, D. C. Schwartz, *Anal Chem* **2004**, *76*, 5293.
[11] D. C. Schwartz, X. H. Li, S. P. Ramnarain, E. J. Huff, Y. K. Wang, *Science* **1993**, *262*, 110.
[12] J. Lin, R. Qi, C. Aston, J. Jing, T. S. Anantharaman, B. Mishra, O. White, M. J. Daly, K. W. Minton, J. C. Venter, D. C. Schwartz, *Science* **1999**, *285*, 1558.
[13] B. Teague, M. S. Waterman, S. Goldstein, K. Potamousis, S. Zhou, S. Reslewic, D. Sarkar, A. Valouev, C. Churas, J. M. Kidd, S. Kohn, R. Runnheim, C. Lamers, D. Forrest, M. A. Newton, E. E. Eichler, M. Kent-First, U. Surti, M. Livny, D. C. Schwartz, *Proc Nat Acad Sci USA* **2010**, *107*, 10848.
[14] Y. Dong, M. Xie, Y. Jiang, N. Xiao, X. Du, W. Zhang, G. Tosser-Klopp, J. Wang, S. Yang, J. Liang, W. Chen, J. Chen, P. Zeng, Y. Hou, C. Bian, S. Pan, Y. Li, X. Liu, W. Wang, B. Servin, B. Sayre, B. Zhu, D. Sweeney, R. Moore, W. Nie, Y. Shen, R. Zhao, G. Zhang, J. Li, T. Faraut, J. Womack, Y. Zhang, J. Kijas, N. Cockett, X. Xu, S. Zhao, J. Wang, W. Wang, *Nat Biotech* **2013**, *31*, 135.
[15] J. O. Tegenfeldt, C. Prinz, H. Cao, S. Y. Chou, W. W. Reisner, R. Riehn, Y. M. Wang, E. C. Cox, J. C. Sturm, P. Silberzan, R. H. Austin, *Proc Natl Acad Sci USA* **2004**, *101*, 10979.
[16] W. W. Reisner, K. J. Morton, R. Riehn, Y. M. Wang, Z. Yuan, M. Rosen, J. C. Sturm, S. Y. Chou, E. Frey, R. H. Austin, *Phys. Rev. Lett.* **2005**, *94*, 196101.
[17] K. D. Dorfman, S. B. King, D. W. Olson, J. D. P. Thomas, D. R. Tree, *Chem Rev* **2012**, *113*, 2584.
[18] R. Riehn, M. Lu, Y.-M. Wang, S. F. Lim, E. C. Cox, R. H. Austin, *Proc Natl Acad Sci U A* **2005**, *102*, 10012.
[19] H. Zohar, S. J. Muller, *Nanoscale* **2011**, *3*, 3027.
[20] L. K. Nyberg, F. Persson, J. Berg, J. Bergström, E. Fransson, L. Olsson, M. Persson, A. W. Stalnacke, J. O. Tegenfeldt, F. Westerlund, *Biochem Bioph Res Co* **2012**, *417*, 404.
[21] A. N. Nilsson, G. Emilsson, L. K. Nyberg, C. Noble, L. S. Stadler, J. Fritzsche, E. R. B. Moore, J. O. Tegenfeldt, T. Ambörnsson, F. Westerlund, *Nucleic Acids Res* **2014**, *42*, e118.
[22] H. Cao, A. Hastie, D. Cao, E. Lam, Y. Sun, H. Huang, X. Liu, L. Lin, W. Andrews, S. Chan, S. Huang, X. Tong, M. Requa, T. Anantharaman, A. Krogh, H. Yang, H. Cao, X. Xu, *Giga Sci.* **2014**, *3*, 34.
[23] L. Schermelleh, I. Solovei, D. Zink, T. Cremer, *Chromosome Res* **2001**, *9*, 77.
[24] A. Tedeschi, G. Wutz, S. Huet, M. Jaritz, A. Wuensche, E. Schirghuber, I. F. Davidson, W. Tang, D. A. Cisneros, V. Bhaskara, T. Nishiyama, A. Vaziri, A. Wutz, J. Ellenberg, J.-M. Peters, *Nature* **2013**, *501*, 564.
[25] Y. Viero, Q. He, L. Mazenq, H. Ranchon, J. Y. Fourniols, A. Bancaud, *Microfluid. Nanofluidics* **2012**, *12*, 465.
[26] Q. He, H. Ranchon, P. Carrivain, Y. Viero, J. Lacroix, E. Darran, J. M. Victor, A. Bancaud, *Macromolecules* **2013**, *46*, 6195.
[27] J. F. Allemand, D. Bensimon, L. Jullien, A. Bensimon, V. Croquette, *Biophys. J.* **1997**, *73*, 2064.
[28] M. Méchali, *Nat. Rev Mol Cell Biol* **2010**, *11*, 728.
[29] J.-W. Yeh, A. Taloni, Y.-L. Chen, C.-F. Chou, *Nano Lett.* **2012**, *12*, 1597.
[30] S. Tuduri, H. Tourrière, P. Pasero, *Chromosome Res* **2010**, *18*, 91.
[31] A. B. Loveland, S. Habuchi, J. C. Walter, A. M. van Oijen, *Nat Methods* **2012**, *9*, 987.
[32] H. Yardimci, A. B. Loveland, A. M. van Oijen, J. C. Walter, *Methods* **2012**, *57*, 179.
[33] V. Bianchi, E. Pontis, P. Reichard, *J Biol Chem* **1986**, *261*, 16037.
[34] C. Lundin, K. Erixon, C. Arnaudeau, N. Schultz, D. Jenssen, M. Meuth, T. Helleday, *Mol Cell Biol* **2002**, *22*, 5869.
[35] C. Carisson, M. Johnson, B. Åkerman, *Nucl Acids Res* **1995**, *23*, 2413.
[36] J. Herrick, A. Bensimon, *Biochimie* **1999**, *81*, 859.
[37] J. N. Bianco, J. Poli, J. Saksouk, J. Bacal, M. Joao Silva, K. Yoshida, Y.-L. Lin, H. Tourrière, A. Lengronne, P. Pasero, *Methods* **2012**, *57*, 149.
[38] S. Oikawa, S. Kawanishi, *Biochim. Biophys. Acta BBA - Gene Struct. Expr.* **1998**, *1399*, 19.
[39] K. H. Rasmussen, R. Marie, J. M. Lange, W. E. Svendsen, A. Kristensen, K. U. Mir, *Lab Chip* **2011**, *11*, 1431.
[40] J. S. Hoffmann, C. Cazaux, *Semin. Cancer Biol.* **2010**, *20*, 312.
[41] T. W. Traut, *Mol. Cell. Biochem.* **1994**, *140*, 1.

[42] M. J. Pillaire, R. Betous, C. Conti, J. Czaplicki, P. Pasero, A. Bensimon, C. Cazaux, J. S. Hoffmann, *Cell Cycle* **2007**, *6*, 471.
[43] Q. He, S. Severac, H. Hajjoul, Y. Viero, A. Bancaud, *Langmuir* **2011**, *27*, 6598.

graphical table of contents (TOC) entry

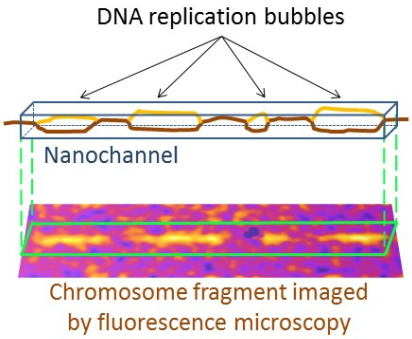

Figure 1

Lacroix et al., 2016

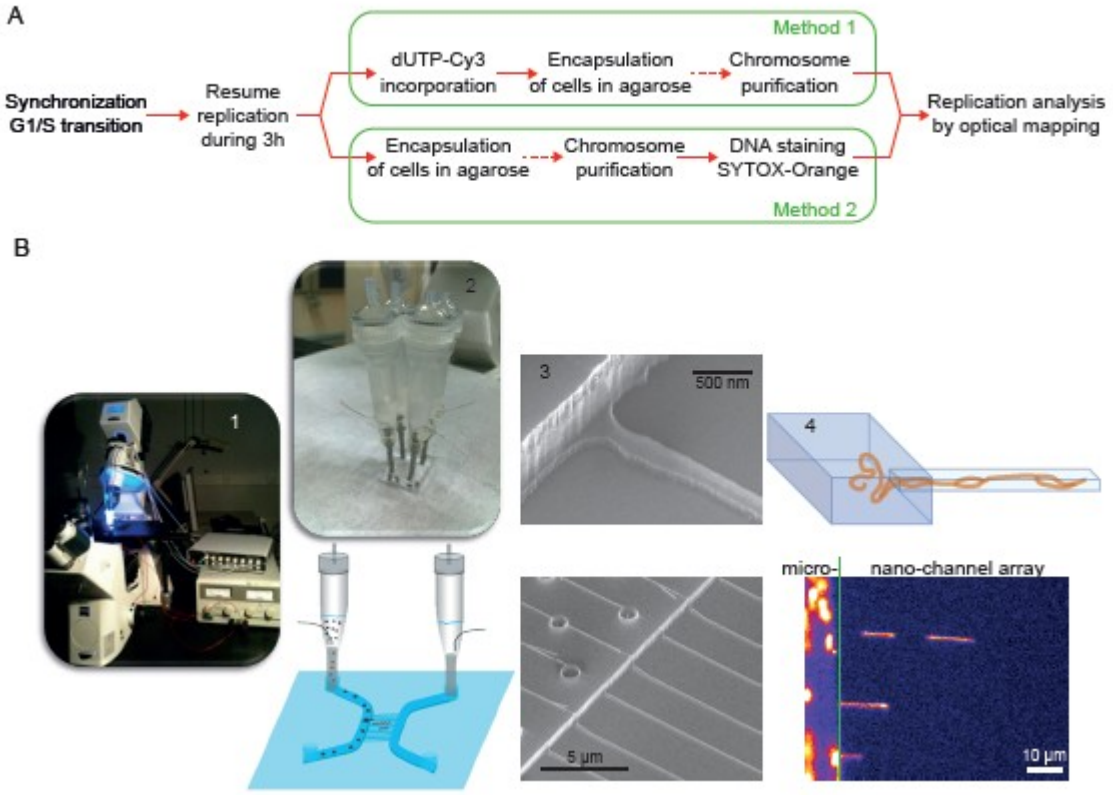

Figure 2

Lacroix et al., 2016

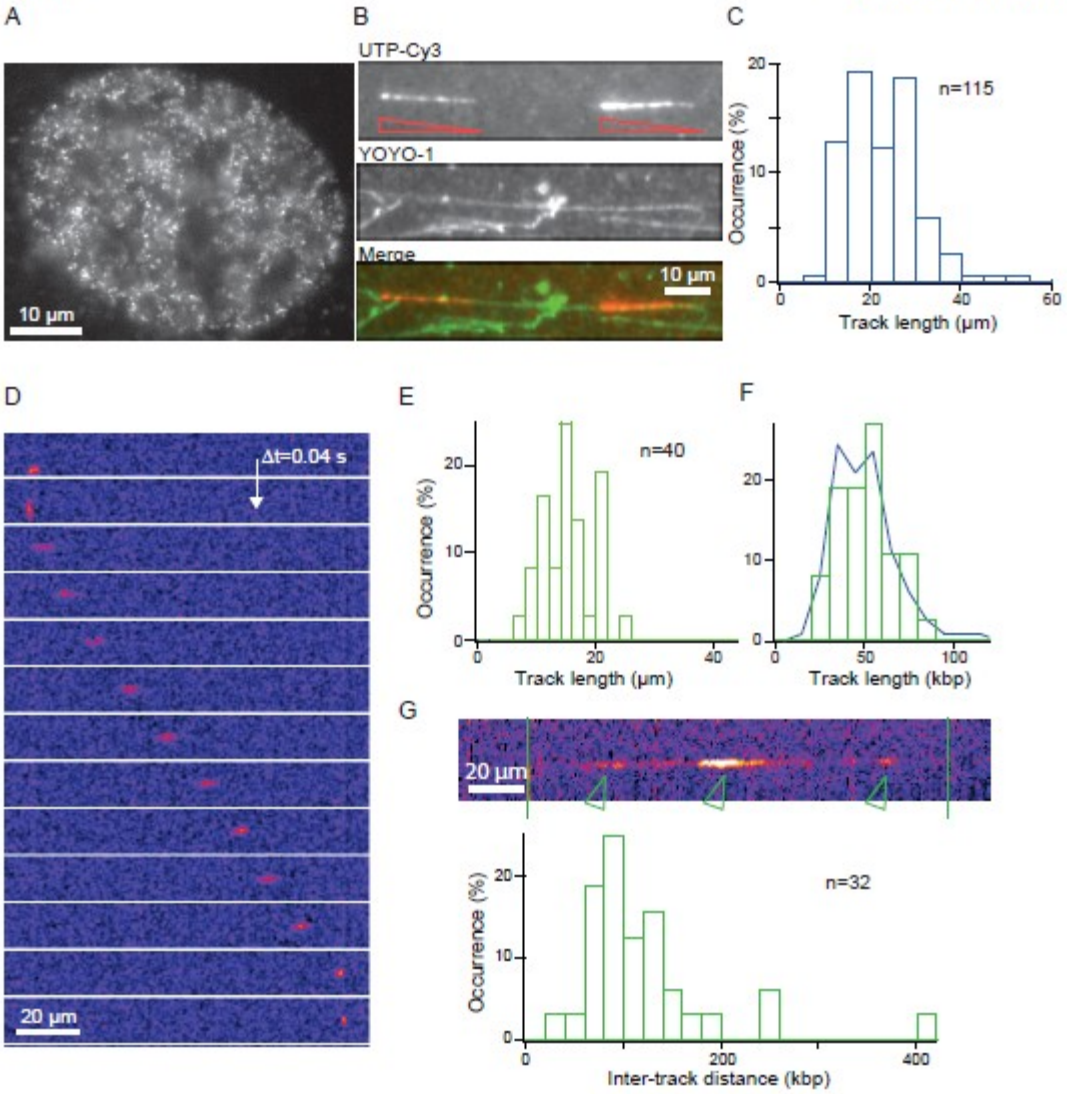

Figure 3

Lacroix et al., 2016

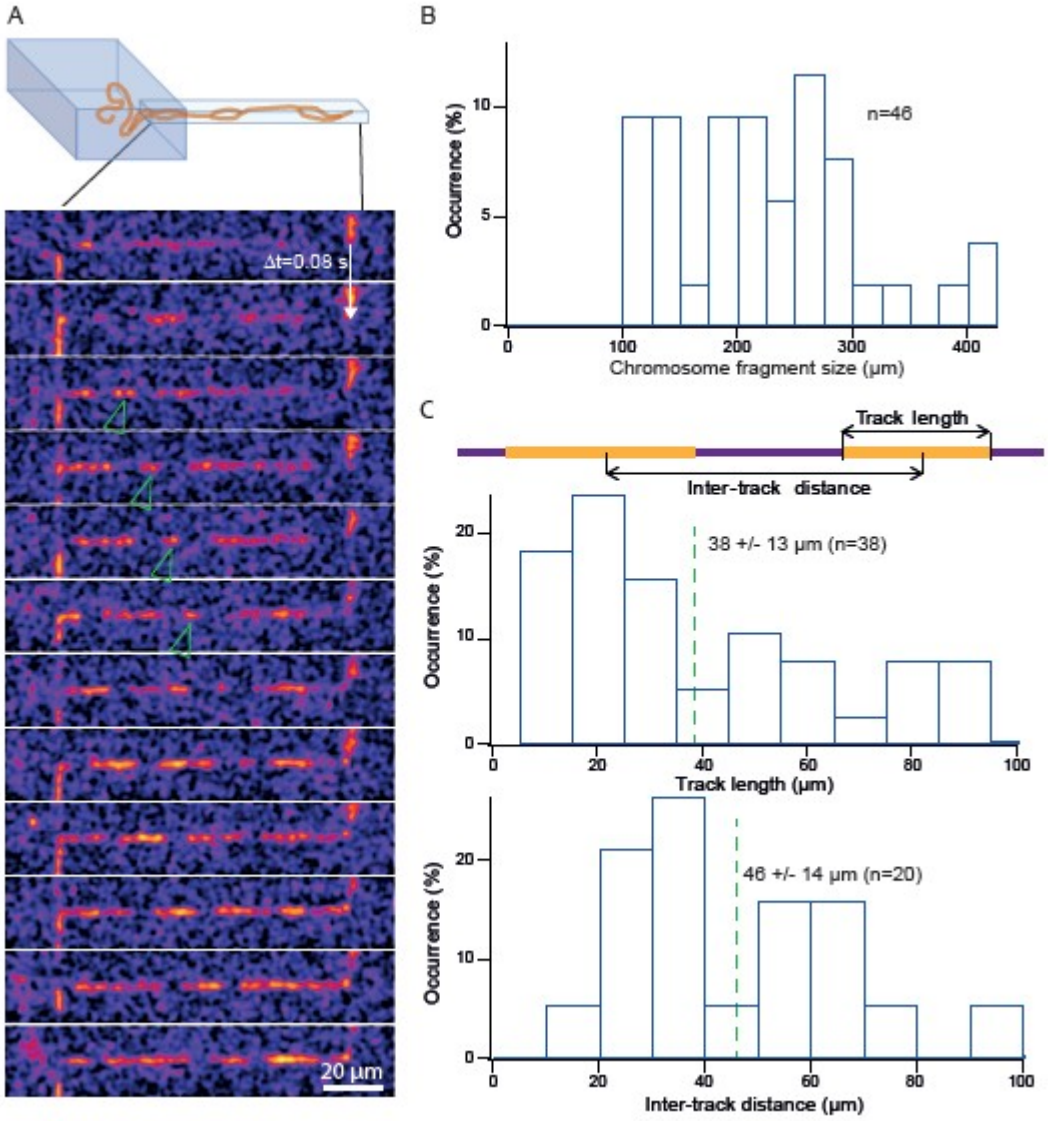

Figure 4 Lacroix et al., 2016

A

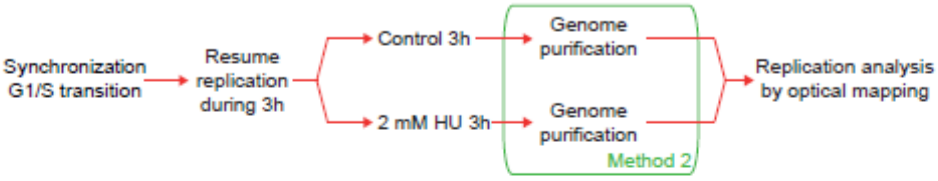

B